Soil Biology and Biochemistry 153 (2021) 107963

Contents lists available at ScienceDirect

Soil Biology and Biochemistry

journal homepage: http://www.elsevier.com/locate/soilbio

Co-occurring increased phosphatase activity and labile P depletion in the rhizosphere of *Lupinus angustifolius* assessed with a novel, combined 2D-imaging approach

Christina Hummel [a,1], Gustavo Boitt [b,1], Jakob Santner [c,*], Niklas J. Lehto [d], Leo Condron [d], Walter W. Wenzel [a]

[a] Department of Forest and Soil Sciences, Institute of Soil Research, University of Natural Resources and Life Sciences Vienna, Tulln, Austria
[b] UWA School of Agriculture and Environment, The University of Western Australia, 35 Stirling Highway, Crawley, WA, 6009, Australia
[c] Department of Crop Sciences, Institute of Agronomy, University of Natural Resources and Life Sciences Vienna, Tulln, Austria
[d] Agriculture and Life Sciences, Lincoln University, Lincoln, New Zealand

ARTICLE INFO

Keywords:
Rhizosphere processes
Diffusive gradients in thin films
Zymography
In situ imaging

ABSTRACT

Innovative non-destructive 2D imaging methods such as zymography and diffusive gradients in thin films (DGT) have been developed recently to assess the distribution of phosphatase activity and labile solutes at the root-soil interface. We report on the first combination of these techniques for the spatial distribution and potential interaction of labile phosphorus (P) and associated acid phosphatase activity in the rhizosphere of blue lupin (*Lupinus angustifolius*) in two contrasting soils ('Sand' and 'Loam'). Zymography, based on 4-methylumbelliferyl-phosphate (MU-P) for acid phosphatase activity mapping, and DGT gels capable of binding labile P were deployed to individual root axes to visualise P mobilisation and depletion in the rhizosphere of blue lupin grown in rhizotrons in glasshouse conditions for 45 days. Acid phosphatase activity was evidently higher in the rhizosphere and co-occurred with P-depletion zones around the roots in both soils. Lateral root profiles showed that elevated acid phosphatase activity as well as P-depletion extended up to 2 mm from the root centre into the rhizosphere. Despite larger total and organic P pools in the Loam, P was less plant available (DGT labile P) than in the Sand. However, phosphatase activities in the rhizosphere and plant P contents were similar in both soils. These results indicate that enzyme-catalysed hydrolysis of organic P was limited in the Loam, due to low P availability, hence explaining similar P contents in lupins from both soils. P did not accumulate in labile pools in the rhizosphere indicating that P supply via phosphatase could not compensate the plants demand for P resulting in P depletion zones. While our work demonstrates the applicability of combined zymography and DGT deployments to study rhizosphere processes at microscale, we also discuss limitations and perspectives of this approach.

1. Introduction

Worldwide, inorganic forms of phosphorus represent only about 57% of total soil P, while the rest is mainly present in organic P forms, especially as phosphate monoesters which account for 33% of total soil P (Menezes-Blackburn et al., 2018). Mineralisation of soil organic P to plant-available phosphate is an important source of P for plants (George et al., 2018; Menezes-Blackburn et al., 2018; Nash et al., 2014; Shen et al., 2011). Plant roots and microorganisms secrete extracellular phosphatases to release P from these monoesters via enzyme-catalysed hydrolysis (George et al., 2018). Legumes are well known for their association with N-fixing bacteria and their ability to take up P from less labile pools (Mat Hassan et al., 2012) and further promote uptake in subsequent crops (Nuruzzaman et al., 2005a). Understanding the functionality of phosphatase enzymes and how they are linked to organic P dynamics and P bioavailability is crucial to improve our understanding of how plant-soil-microbial interactions affect plant nutrition (George et al., 2018).

Zymography is a relatively new technique to visualise the spatial distribution of potentially active enzymes in soil with 2D images (Spohn et al., 2013). It is based on the visualisation of substrates that become

* Corresponding author.
E-mail address: jakob.santner@boku.ac.at (J. Santner).
[1] Two first authors contributed equally to this work.

https://doi.org/10.1016/j.soilbio.2020.107963
Received 15 April 2020; Received in revised form 3 August 2020; Accepted 16 August 2020
Available online 25 August 2020

Abbreviations

DGT	diffusive gradients in thin films
MU-P	4-Methylumbelliferyl phosphate
MU	4-Methylumbelliferone

fluorescent after reaction with substrate-specific enzymes (Spohn et al., 2013). The technique allows non-destructive investigations of enzyme dynamics in soils (Heitkötter and Marschner, 2018) and rhizospheres *in situ* (Ma et al., 2018b, 2018a; Razavi et al., 2016). Phosphatase activity is generally higher in the rhizosphere compared to bulk soil, as it is either directly released by roots or by microorganisms that are stimulated by rhizodeposits (Kuzyakov and Razavi, 2019). However, distribution of the enzyme activity depends on plant species (Razavi et al., 2016) and growth (Ma et al., 2018a), and can vary within the root system due to rhizosphere processes and functions (Razavi et al., 2016), including the quality and quantity of root exudates (Zhang et al., 2019). The efficacy of phosphohydrolases to mobilise organic P strongly depends on soil physical and chemical characteristics like texture and soil pH, which affect sorption, proteolysis and inactivation of enzymes (George et al., 2005; Menezes-Blackburn et al., 2018). Moreover, while rhizosphere microorganisms can contribute to this mobilisation through enzyme release, they can also compete with roots by immobilizing P in their biomass (Kuzyakov and Razavi, 2019; Mat Hassan et al., 2012).

Phosphorus uptake and depletion along roots has been demonstrated using ^{33}P-labelled soil and autoradiography (Bhat and Nye, 1973). More recently, a multi-analyte solute imaging technique coupling diffusive gradients in thin films (DGT) gels with laser-ablation inductively coupled plasma mass spectrometry (LA-ICP-MS) has been developed to assess the heterogeneity of nutrient availability and the impact of root activities on nutrient depletion and mobilisation along individual root axes across a planar interface (Kreuzeder et al., 2018, 2013; Santner et al., 2012). In contrast to autoradiography that measures total P irrespective of its bonding in soil, these two-dimensional (2D) DGT measurements can show the spatial distribution of labile cations and anions in soil solution (Santner et al., 2012). DGT images represent fluxes of readily bio-available P and cations such as iron, copper, zinc, and manganese (Kreuzeder et al., 2013). The masses of these ions bound at different locations in the gel reflect how much can be resupplied to the DGT probe interface by the soil at these locations. Labile phosphorus accumulated on DGT gels can be supplied by diffusion and desorption from labile solid phases, and processes linked to biological activity, such as release of P from organic pools (organic P) by enzymes, or dissolution of P-binding minerals by root/microbial exudates. Santner et al. (2012) observed depletion zones of labile P around two *Brassica napus* L. cultivars and also showed increased labile P near root tips of one of the cultivars, which they linked to P efflux and P mobilisation by localised organic acid anions or proton exudation. They demonstrated that visualisation of soil solution depletion and nutrient release from roots can provide new insights into nutrient uptake and P mobilisation mechanisms in rhizospheres, which can include the effect of phosphatase enzymes.

Imaging techniques at the sub-mm scale enable direct observation of physico-chemical and microbial processes involved in P cycling in soils, which provides fundamental information for effective and sustainable management of P resources in agriculture (George et al., 2018). Yet, there have been no attempts to combine zymography and DGT to link phosphatase activity and P dynamics in the rhizosphere. The primary objective of this study was to introduce the first combination of zymography and DGT imaging, and to discuss the merits and limitations of this approach. To this end, we conducted a case study to quantify localized mechanisms of P mobilisation and associated phosphatase activity in the rhizosphere of blue lupin (*Lupinus angustifolius* L.). grown on two soils with contrasting texture. As a secondary objective we explored the results of this case study to identify processes of P biogeochemistry in the rhizosphere to demonstrate the added value of the combined approach. By addressing the two research questions we hypothesized (1) that the combined approach would be feasible and provide additional information compared to the application of the individual techniques, and more specifically, that in both soils (2a) acid phosphatase activity is increased along roots compared to bulk soil, (2b) root and microbial uptake cause P depletion zones around the roots and (2c) phosphatase-induced mineralisation of organic P increases the labile P pool.

2. Materials and methods

2.1. Soils

Two contrasting soils were selected for this study. The sandy soil (forthwith "Sand"), was collected from a coastal dune near Haast, New Zealand and was slightly more acidic (pH_{H2O} 5.6; Table 1) than the other soil. It developed on unconsolidated sand, had no horizons and is classified as Eutric Arenosol according to the World Reference Base for Soil Resources (WRB). The vegetation cover was lowland, mixed conifer–broadleaf temperate rainforest with woody angiosperms and tree ferns (Turner et al., 2012). The second soil was a shallow loam soil collected near Omarama Township, New Zealand (forthwith "Loam"). It was a young soil that formed on alluvial sediments, classified as Skeletic Cambisol (Dystric, Loamic) according to WRB. It was covered by grassland, i.e. *Agrostis capillaris*, *Trifolium arvense*, *Pilosella officinarum* (Whitley et al., 2016; Hendrie et al., 2018). It was more basic (pH_{H2O} 6.3) and had the higher total and organic P content compared to the Sand (Table 1). Both soils were sampled from the upper 20 cm, air dried and sieved < 2 mm.

Soil P fractionation was conducted according to Condron et al. (1996) as modified by Boitt et al. (2018) to characterise the P pool distribution. Briefly, 0.5 g of soil (<2 mm) were extracted sequentially with the following extractants (10 mL): 1 M ammonium chloride (NH_4Cl), 0.5 M sodium bicarbonate ($NaHCO_3$, pH 8.5), 0.1 M sodium hydroxide (NaOH–I), 1 M hydrochloric acid (HCl) and 0.1 M sodium hydroxide (NaOH-II), and digestion of the soil residue with concentrated sulfuric acid and hydrogen peroxide (30% v/v) (Residual P). Inorganic P was measured in an aliquot of the extraction solution by colorimetry of molybdate reactive P (Dick and Tabatabai, 1977) and total P measured after persulfate and sulfuric acid digestion of each extract in an autoclave. The difference between total P and molybdate reactive P (i.e. the molybdate unreactive P) was considered as an approximation of the

Table 1
Selected soil properties.

		Sand	Loam	p-value
Texture	sand (g kg^{-1})	986	545	
	silt (g kg^{-1})	<10	359	
	clay (g kg^{-1})	14	93	
pH (H_2O)		5.58 ± 0.15	6.20 ± 0.03	*
C_{org}	g kg^{-1}	9.14 ± 0.16	31.1 ± 0.00	**
N	g kg^{-1}	0.86 ± 0.03	2.74 ± 0.10	*
C: N		10.7 ± 0.16	11.3 ± 0.40	
P total	mg kg^{-1}	99.7 ± 1.78	899 ± 5.45	***
inorganic P (P_i)	mg kg^{-1}	42.3 ± 1.78	377 ± 6.89	***
organic P (P_o)	mg kg^{-1}	42.0 ± 0.61	381 ± 1.18	***
residual P	mg kg^{-1}	15.5 ± 0.53	141 ± 0.91	
P_i: P_o		1.01 ± 0.03	0.99 ± 0.02	

Inorganic P represents the sum of molybdate-reactive P fractions in sequential NH_4Cl, $NaHCO_3$, NaOH–I, HCl and NaOH-II extracts, while organic P represents the difference between inorganic P and total P in each extractant. Values represent mean ± standard error. Significant differences between means are indicated by asterisks, where * $p < 0.1$, ** $p < 0.01$, *** $p < 0.001$ (Student's t-test, $n = 3$).

organic P. The sum of $NaHCO_3$, NaOH–I and NaOH-II extractable organic P was considered as total extractable organic P, whereas the sum of inorganic P in all extracted fractions (NH_4Cl, $NaHCO_3$, NaOH–I, HCl and NaOH-II) was regarded as total extractable P_i. Total soil P is given by the sum of all extracted fractions plus residual P. Carbon and nitrogen content were analysed by an elemental analyser (Vario-Max CN Elemental Analyser, Elementar Australia Pty. Ltd), the soil C is considered here to be exclusively in organic forms (Tate et al., 1997).

2.2. Rhizotron experiment

Blue lupin (*Lupinus angustifolius* L.) was grown under greenhouse conditions (19 ± 3 °C) in flat growth containers (rhizotrons) with inner dimensions of 15 × 30 × 2.5 cm and a detachable plate. The two soils were packed in the rhizotrons to achieve a bulk density of 1.4 and 1.0 g cm^{-3} in the Sand and the Loam, respectively. The rhizotrons were kept at an angle of 45° to encourage roots to grow along the downward-facing detachable plate. Gravimetric water content in the rhizotrons was maintained at 80% of field capacity by weighing. After 45 days the rhizotrons were brought to the laboratory for analyses as described below. Triplicates for each soil type were set up in a completely randomised arrangement. After the experiment, the plant shoots were harvested, dried, and weighed to quantify the shoot biomass. The rhizosphere soil was collected by very gently removing the roots from the soil in the rhizoboxes and then collecting the remaining soil attached to the roots. Soil pH was determined in water extracts of rhizosphere and bulk soil (soil:water 1:2.5 v/v). The dried shoots were ground and digested in HNO_3 and H_2O_2 using microwave digestion (MARSXPRESS, CEM Corp.). The digests were analysed using optical emission spectrometry (ICP-OES, Varian 720 ES – USA). Analyte recovery was confirmed through analysis of a certified reference material (NIST Tomato leaf 1573).

2.3. Visualisation of phosphatase activity by zymography

The *in situ* measurement of acid phosphatase distribution was conducted for 40 min. We followed the procedure of Giles et al. (2018) and Spohn et al. (2013). Nylon filter membranes (0.45 μm pore size, 12.5 cm diameter; Whatman 7404–009, GE Healthcare, UK) were prepared for the zymography imaging within 16 h before deployment. They were soaked in 6 mM 4-Methylumbelliferyl-phosphate (MU-P) disodium salt (Sigma-Aldrich, no. M8168) for 10 min and then dried for further 10 min at 30 °C. The MU-P solution was prepared with 40 mM modified universal buffer adjusted to a pH of 6.5. The detachable lower plate from each rhizotron was opened in turn and covered with Nuclepore membrane (Nuclepore Track-Etched Membrane 0.2 μm, Whatman, UK). A ~1 mm thick agarose gel (1% w/v, also prepared in 40 mM modified universal buffer at pH 6.5, prepared within 16h prior application) was placed on the membrane and acted as the mobile phase for the substrate. The pre-prepared MU-P impregnated filters were laid on the agarose gel, covered with aluminium foil, and incubated for 40 min under laboratory conditions (20 °C). During deployment, the MU-P substrate diffused from the filter to the soil where acid phosphatases catalyse its hydrolysis to phosphate and 4-methylumbelliferone (MU) that fluoresces under UV light. The MU then diffuses back to the filter membrane (Razavi et al., 2019). At the same time, enzymes from the soil surface possibly also diffuse towards the membrane and induce MU fluorescence. However, during the relatively short deployment time of zymography filters, the diffusivity of MU-P is much higher compared to phosphatases due to its much smaller hydrodynamic radius and the associated higher diffusion coefficient (Razavi et al., 2019). After the deployment, filters were dried for 4 min at 30 °C in an oven and photographed under UV light (365 nm) in an UVP DigiDoc-It imaging system (UVP, Upland, California, USA) comprised of a lightweight hood with UV blocking viewport and an UV transilluminator. Images were recorded with a Canon Powershot G7 10 MP digital camera equipped with a 6x image-stabilized optical zoom (Canon, Tokyo, Japan) which was connected to a computer and controlled using a capture software (Doc-ItTMLS version 6.3.3, UVP, California, USA). Exposure time was 1 s. The spatial distribution of the fluorescence intensity on the filter shows the quantity of MU released by enzymatic hydrolysis of MU-P, which can be interpreted as phosphatase activity per unit area and time. The resulting resolution was 65 μm. Zymography calibration standards were prepared according to Giles et al. (2018) by soaking 4 cm^2 filter papers in solutions with known concentrations of fluorescent 4-methylumbelliferone (MU). We chose to fit a saturation calibration curve with MS Excel Solver (Office 365) as the grey value intensity slightly levelled off with higher MU concentrations (see supporting information). The fitting constants GV_{max} and k were determined by fitting grey values (GV) with the activities from the calibration curve calculated with the MU concentration and to the incubation time, given in pmol mm^{-2} h^{-1}. The grey value from the calibration blank (a membrane immersed in buffer without fluorescent MU, *blank)* was added as the intercept to conduct the background correction.

$$GV = GV_{max} * \left(1 - exp^{(-k*activity)}\right) + blank$$

Grey values in the zymograms were transformed to activities with this function:

$$Activity = \log\left(1 - \frac{GV - blank}{GV_{max}}\right) * \frac{1}{-k}$$

2.4. Visualisation of labile cations and anions by diffusive gradients in thin films

Following the zymography assessments the moisture content of the soils was increased to maximum water holding capacity with distilled water 24 h prior to deploying the DGT gels for another 24 h on specific regions of interest (ROI) within the area previously analysed by zymography. These ROIs were selected with a focus on targeting the tips of the lupin roots. The rhizotrons of each soil are presented in Fig. 1 with the corresponding zymogram and the region targeted for the DGT deployments.

Diffusive gradients in thin film (DGT) gels capable of binding labile cations and anions were prepared as described by Kreuzeder et al. (2013). The cation resin SPR-IDA (suspended particulate reagent-iminodiacetate, CETAC Technologies, Nebraska, US) and the anion resin zirconium hydroxide precipitate were embedded in a polyurethane-based hydrogel matrix (HydroMed-D4, AdvanSource biomaterials, Massachusetts, US). For the soil deployment, DGT gels were mounted on detachable plates and overlain with Nuclepore membrane. After the deployment, the assembly was carefully rinsed with a jet of high-purity water. The Nuclepore membrane was removed and the gel was mounted onto a filter paper, ensuring geometric integrity of the gel. The gels were then dried using a gel dryer for 12 h at 60 °C. DGT calibration standards for laser-ablation inductively coupled mass spectrometry (LA-ICPMS) were prepared by immersing resin-gel disks assembled in DGT samplers in deployment solutions containing different concentrations of P in quadruplicates. The analyte quantities taken up by the resin gel were determined on three gel replicates by sectorfield-ICPMS (Thermo Fisher ELEMENT XR (Thermo Fisher Scientific, Bremen, Germany) after microwave-assisted digestion with HNO_3 and H_2O_2. The fourth standard gel was dried in a gel drier and analysed together with the sample gels and a sample blank gel by LA-ICPMS.

LA-ICPMS was performed on one DGT gel per soil as one DGT region of interest comprised several root tips and features visualised by DGT at specific positions have shown a good replicability (e.g. Wagner et al., 2020). LA-ICPMS was conducted in line scanning mode using a UP 193-FX (ESI, NWR Division, Portland, USA) laser ablation system coupled to an ELAN 9000 DRCe quadrupole ICPMS (PerkinElmer, Wallthan, MA). Helium was used as the LA carrier gas (flow rate of 900 mL min^{-1}). This He gas stream was mixed with the ICPMS Ar nebulizer gas stream prior to introduction into the ICPMS. The diameter of the

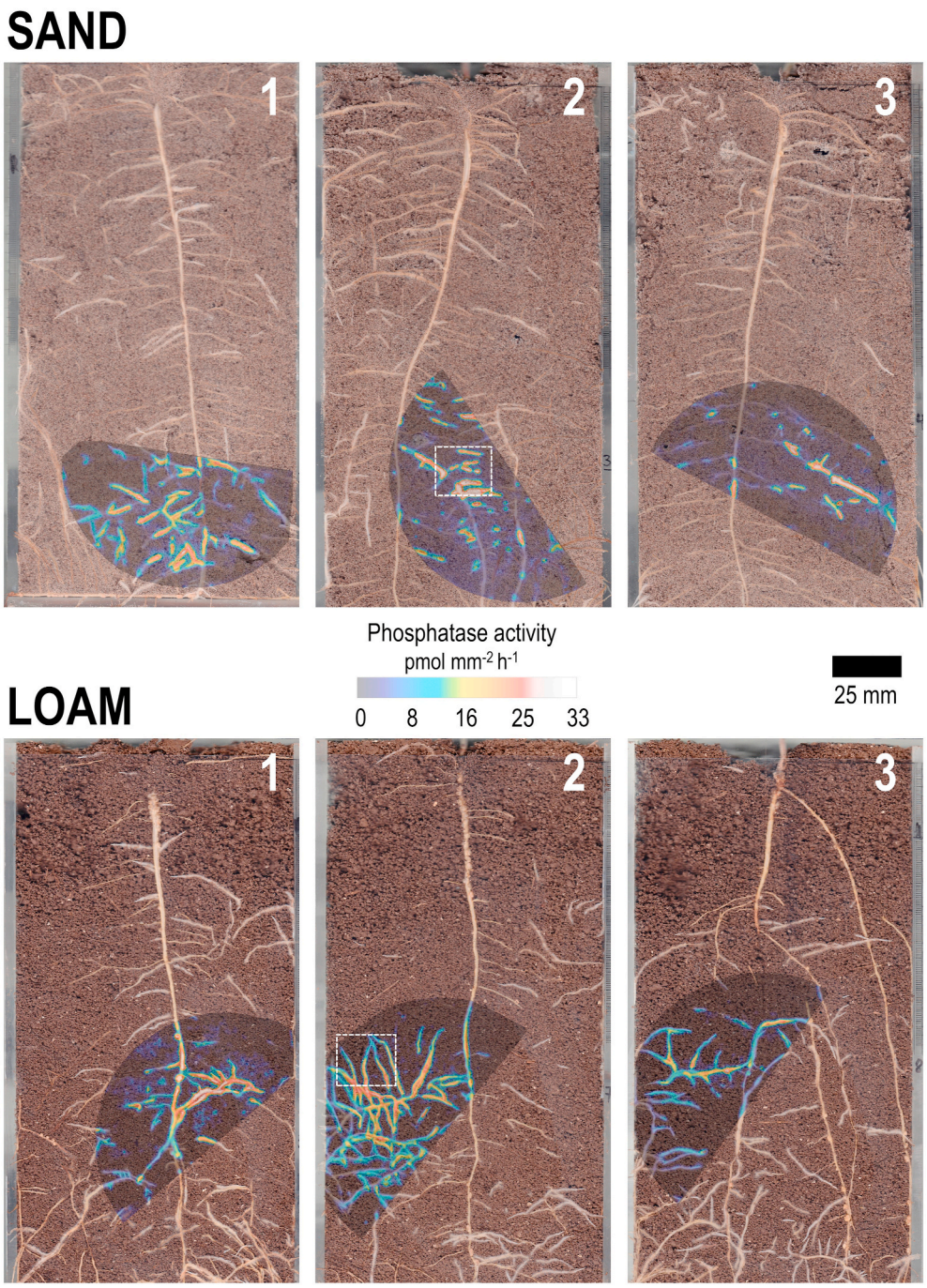

Fig. 1. Rhizothrons of the Sand (top) and the Loam (bottom) with zymograms displayed as transparent overlay and DGT region of interest (white dashed rectangles). Increasing phosphatase activity is indicated by red/yellow colour. (For interpretation of the references to colour in this figure legend, the reader is referred to the Web version of this article.)

laser beam was 150 μm and the scan speed across the gel was 300 μm s^{-1}. The laser fluency at the sample was 2.1 J cm^{-2}. The scan direction was perpendicular to the roots and the interline distance was 400 μm. The ICPMS method was set to scan for ^{13}C, ^{31}P, ^{51}V, at a scan cycle time of 0.33 s. The resulting resolution in scan direction (perpendicular to the roots) was 99 μm and 400 μm along the roots. The sample counts (intensity) were corrected for the gas blank signal and normalized to the ^{13}C signal, which was used as internal standard. The vanadium (^{51}V) signal was used to indicate DGT-soil contact and identify air bubbles, that should be excluded from image analysis. Means of 150 corrected readings from the sample blank gel and standard gels were plotted against the average loadings of the 3 digested gel standard replicates to produce a calibration curve. The mass accumulated on the DGT sample gel was corrected for the average mass of the sample blank and expressed as an average flux during the DGT deployment time (pg cm^{-2} s^{-1}). The LOD and LOQ were calculated from the signal of the sample gel blank as 3 and 10 times the standard deviation (SD) of the mean signal, respectively.

2.5. Image processing

Root photographs, DGT images and zymograms were brought to the same size (without interpolations) in ImageJ Fiji (Schindelin et al., 2012) and aligned in Photoshop (CS5, V12.0, Adobe Systems

Incorporated, 2010) with the help of photographs during the application. Templates (e.g. angle for rotation and coordinates for alignment) created in Photoshop were used to crop the original images and conduct analysis of the same sections in ImageJ Fiji.

2.6. Image analysis

The images from all zymograms (3 replicates/soil) were included in the analysis, while DGT images were from the single rhizosphere ROIs (1 replicate/soil). Background acid phosphatase activities were calculated as the average of three 1 cm^2 areas per zymogram, (n = 9 per soil) away from any obvious root structures (*i.e.* the bulk soil). Likewise, the background P flux was determined in four 0.25 cm^2 areas in the DGT images. 'Hotspots' of phosphatase activity in each soil were defined as areas where the activity was three standard deviations above the average background for that soil (Razavi et al., 2019). Mean phosphatase activity in hotspot area and mean rhizosphere P depletion were measured with the help of thresholds and selections in ImageJ Fiji. The root surface area was estimated by delineating the visible root manually with the polygon tool in ImageJ Fiji, under the assumption that the full width of the analysed root was visible. The extent of phosphatase activity and P flux alteration in the rhizosphere was analysed with the help of lateral root profiles across 3 roots per soil within the DGT-ROI in ImageJ Fiji. The root images were straightened to facilitate profile drawing across and along crooked roots. Data were collected from areas with dimensions of 1 x 6–8 mm across the roots at the tip and in the root hair zone (1–2 cm from the tip, depending on root length in the ROI and clearly visible root hairs). Profiles along the same roots were taken at the root surface and within the first mm in the rhizosphere at both sides of the root. Moreover, profiles along 8 lateral roots per box were averaged to investigate phosphatase activity along roots.

2.7. Statistical analysis

Student's t-tests were conducted in R studio (version 1.1.463, 2018 RStudio, Inc.). In case of heteroscedasticity (established using Levene's test), *t*-test with the Welch approximation to the degrees of freedom was used. Normality of the data was confirmed using Shapiro-Wilk's test. The significance level of $p < 0.01$ was used throughout, unless stated otherwise. Graphs were prepared using Sigma Plot (v. 12.5, Systat Software Inc.).

3. Results

3.1. Soil properties and P fractionation

In line with the differences in texture, in the Loam carbon and nitrogen contents were three times larger than in the Sand, while the C/N ratios were similar in both soils (Table 1). The Sand was more acidic than the Loam, but pH increased in the rhizosphere by 0.75 units tp pH 6.33 ($p < 0.05$, n = 3), whereas no change was observed in the Loam. Rhizosphere pH was similar between the two soils ($p > 0.05$). The total P, inorganic P and organic P concentrations in the Sand were approximately nine times lower than in the Loam ($p < 0.01$; Table 1) and all P fractions were greater in the Loam ($p < 0.01$). The only exception was the NH_4Cl-extractable inorganic P concentration that was significantly higher in the Sand (Table 2). While the sum of NH_4Cl- and $NaHCO_3$-extractable P_i and P_o, which is considered as labile P, was 2.9-times greater, the moderately labile P (i.e. sum of NaOH–I extractable P_i and P_o) was 12 times greater in the Loam than in the Sand. The ratio of total extractable inorganic to organic P was similar for both soils (Table 1).

3.2. Acid phosphatase activity and P flux in blue lupin rhizosphere

In both soils high acid phosphatase activity (zymograms) was associated with P depletion zones (DGT image) along observable roots

Table 2
Soil phosphorus fractionation (P_i = inorganic P; P_o = organic P).

	Sand	Loam	P-value
	mg kg^{-1}	mg kg^{-1}	
P_i NH_4Cl	0.82 ± 0.06	0.13 ± 0.04	**
P_i $NaHCO_3$	3.84 ± 0.16	15.4 ± 0.63	**
P_o $NaHCO_3$	5.78 ± 0.32	14.6 ± 0.59	***
P_i NaOH	4.89 ± 0.36	80.5 ± 0.80	***
P_o NaOH	27.0 ± 0.64	300 ± 2.38	***
P_i HCl	29.8 ± 0.99	229 ± 2.89	***
P_i NaOH II	2.88 ± 0.27	51.8 ± 3.29	**
P_o NaOH II	9.19 ± 0.62	66.9 ± 1.35	***
P residual	15.5 ± 0.53	141 ± 0.91	***

Values represent mean ± SE, p-values result from Student's t-test, n = 3, * $p < 0.1$, ** $p < 0.01$, *** $p < 0.001$.

(Fig. 2). Bulk P flux was 1.44 ± 0.29 and 0.87 ± 0.19 pg cm^{-2} s^{-1} (mean ± SD) in the Sand and in the Loam, respectively. Acid phosphatase activity in the bulk soil was very low with 0.2 ± 1.0 and −1.5 ± 1.3 pmol mm^{-2} h^{-1} in the Sand and Loam, respectively. The hotspots of acid phosphatase were generally associated with visible roots, while P depletion could be observed at roots slightly covered by soil (compare root 1 in soil A in Fig. 2). Phosphatase activity within the hotspots did not significantly differ between the two soils with means of 9.5 ± 6.2 and 9.1 ± 5.5 pmol mm^{-2} h^{-1} in the Sand and Loam, respectively. However, phosphatase hotspots in the Loam were more evenly distributed between most visible roots while in the Sand not all roots showed elevated phosphatase activity and hotspots were locally more pronounced. Generally, there was a two-fold increase in phosphatase activity from the root tips towards the root hair zone; this was up to 2.5 times in the Sand. Zones of P depletion mostly aligned with the visible roots and were at a similarly low level in both soils. P flux directly on the root surfaces was 0.26 ± 0.11 and 0.21 ± 0.08 pg cm^{-2} s^{-1}, in the Sand and the Loam. In both soils, the depletion zone extended 0.9 ± 0.4 mm from the root surface into the soil. Mean P flux within the depletion zone was 0.40 ± 0.22 pg cm^{-2} s^{-1} in the Sand and 0.28 ± 0.12 pg cm^{-2} s^{-1} in the Loam, which was 3.6- and 3.1-times lower compared to the corresponding bulk soil in the Sand and the Loam, respectively.

Profiles across the three roots analysed in the DGT ROI showed that zones of high phosphatase activity extended up to 2 mm from the root centre and corresponded with the P-depletion in the root hair zone of both soils (representative root profiles are shown in Fig. 3a and b). While the results for enzyme activity and P mobilisation were very similar across all roots analysed, the morphology (e.g. start of root hair zone etc.) differed. For this reason, we only show one example profile plot per soil.

The shoot dry weight of lupins grown on the Sand was 1.2 ± 0.1 g (mean ± SE) and significantly higher than that the plants grown on the Loam (0.7 ± 0.1 g). Conversely, shoot P concentration was significantly higher in plants grown on the Loam (1.95 ± 0.13 g kg^{-1}) compared to those grown on the Sand (1.34 ± 0.06 mg kg^{-1}). Consequently, the P content per plant did not differ between the two soils (Table 3).

Plants grown on the Sand had 2.5-, 1.4- and 8.5-times higher sulphur (S), magnesium (Mg), and sodium (Na) concentrations than plants grown on the Loam (Table 3), while P, potassium (K) concentrations were 4 times higher for plants grown in the Loam. Moreover, plants grown in the Loam had also 1.4- and 1.6-times higher iron (Fe) and copper (Cu) concentrations compared to the Sand, respectively.

4. Discussion

4.1. Biomass production of blue lupin in relation to soil properties

Despite the almost 10-fold lower organic and inorganic P content of the Sand, lupin shoot dry weight at termination of the experiment was ~70% higher than in the Loam. This difference in biomass production is

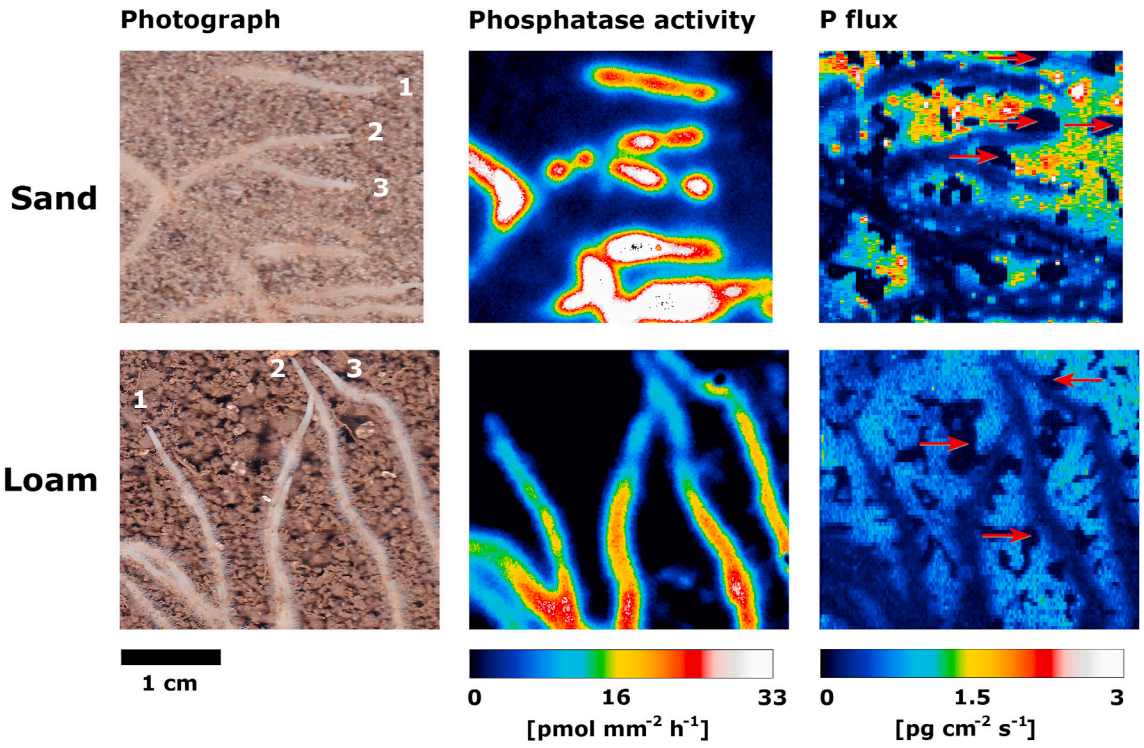

Fig. 2. Root images, zymograms of acid phosphatase activity and DGT-measured P flux in Sand (top) and Loam (bottom). Profiles were taken from the labelled roots (white numbers in the photograph). Examples of air bubbles in the DGT images are marked with red arrows. (For interpretation of the references to colour in this figure legend, the reader is referred to the Web version of this article.)

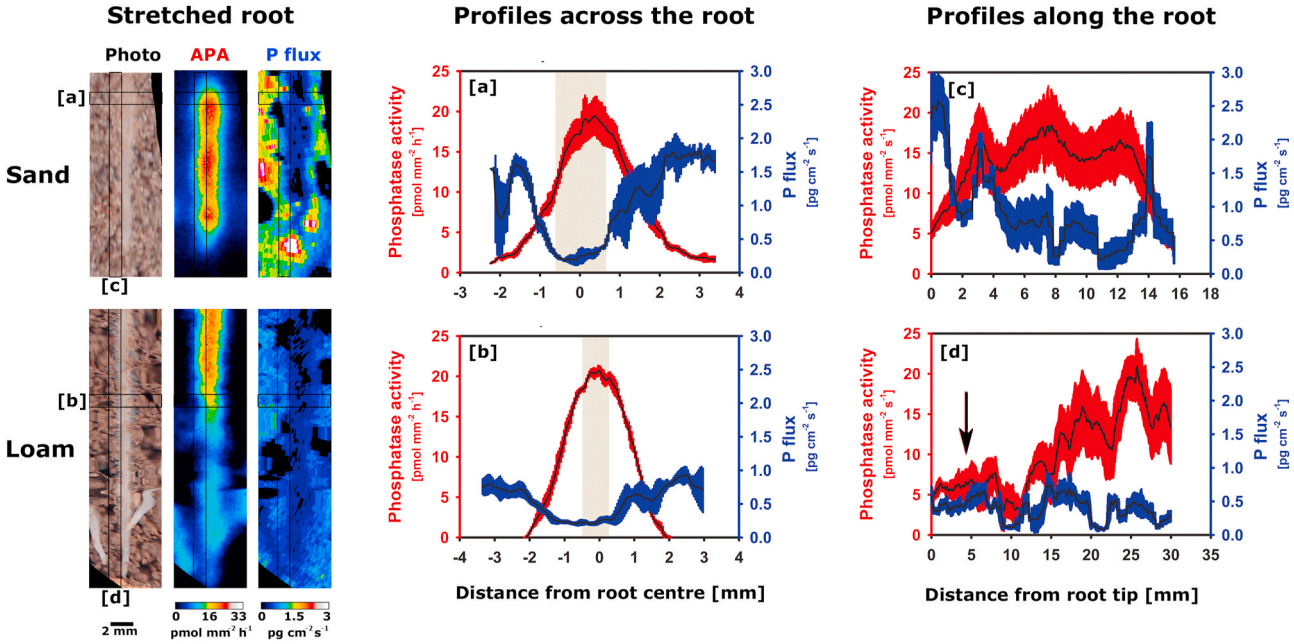

Fig. 3. Acid phosphatase activity and P fluxes around single roots grown in the Sand (top) and Loam (bottom) visualised as profiles across (a and b) and along (c and d) a straightened root. Acid phosphatase activity (APA) is shown in red, on the left y-axis; DGT-measured P flux is shown in blue and on the right y-axis. The central black curves show the mean, while the coloured shading represents the standard deviation within a 1 mm-thick profile. Locations of the profiles are highlighted as black boxes in the root images. Profiles across the root show extents of phosphatase activity and P depletion beyond the root surface, which is shown as brown bar in the centre of the x-axis. The black arrow in figure [d] marks the beginning of the root hair zone, while in [c] this was not visible on the photo but on average the distance between root tip and first root hairs was 4.3 ± 1.9 mm (mean ± standard deviation, n = 60, i.e. 10 roots per rhizotron). (For interpretation of the references to colour in this figure legend, the reader is referred to the Web version of this article.)

likely related to the texture of the Sand, which would have facilitated improved aeration, water availability and mass flow of plant nutrients during the rhizotron experiment. The observed higher shoot concentrations of S, Mg and Na in lupins grown on the Sand support this interpretation, as these nutrients are primarily supplied to roots by mass flow. In contrast, the shoot concentrations of P, Fe and Cu observed in

Table 3
Nutrient uptake of *L. angustifolius*.

	Shoot nutrient concentration			Shoot nutrient content		
	Sand	Loam	P-value	Sand	Loam	P-value
	g kg^{-1}			mg rhizobox^{-1}		
P	1.34 ± 0.06	1.95 ± 0.13	*	1.59 ± 0.08	1.41 ± 0.20	
K	5.54 ± 0.82	21.5 ± 1.26	***	6.42 ± 0.54	15.2 ± 1.54	*
Ca	13.0 ± 0.75	11.5 ± 0.49		15.6 ± 1.85	8.29 ± 1.06	*
Mg	9.32 ± 0.38	6.53 ± 0.20	**	11.2 ± 1.22	4.69 ± 0.57	**
Na	3.39 ± 0.44	0.40 ± 0.03	**	4.07 ± 0.67	0.28 ± 0.02	*
S	2.98 ± 0.09	1.20 ± 0.04	***	3.55 ± 0.24	0.85 ± 0.09	***
	mg kg^{-1}					
Fe	262 ± 24.2	371 ± 26.5	*	0.32 ± 0.05	0.27 ± 0.04	
Zn	95.6 ± 2.50	76.5 ± 11.8		0.11 ± 0.01	0.06 ± 0.01	*
Cu	5.14 ± 0.53	7.91 ± 0.26	**	0.01 ± 0.00	0.01 ± 0.00	
Mn	650 ± 44.4	558 ± 63.4		0.77 ± 0.08	0.41 ± 0.08	*
Mo	0.71 ± 0.09	0.54 ± 0.04		0.86 ± 0.14	0.38 ± 0.05	*
Al	59.3 ± 9.38	65.0 ± 4.98		0.07 ± 0.02	0.05 ± 0.01	

Values represent mean ± SE, p-values result from Student's t-test, n = 4, * $p < 0.1$, ** $p < 0.01$, *** $p < 0.001$.

plants from the Loam were 1.4–1.6 times higher than on the Sand, while there was no significant difference in the shoot contents (shoot concentration x biomass) of these elements, indicating a "dilution" effect on the Sand where lupin plants had a larger shoot biomass. Shoot P concentrations (1.3–2.0 g kg^{-1}) in the soils used in this study were similar to blue lupin plants only 11 days older (1.3–2.7 g kg^{-1}) grown in P-fertilized Sand (Adams and Pate, 1992), suggesting that lupins in the present study were able to cope with P-levels in both experimental soils. However, plant P concentrations were below the critical value of 2.7–3.7 g kg^{-1} for blue lupins <80 days recommended by Scanlan (2015).

DGT-gels bind P present in the soil solution as well as P resupplied from the soil solid phase upon soil solution depletion and hence account for available P. DGT P-flux in the bulk soil was 66% greater in the Sand than in the Loam, even though one might expect larger P resupply rates based on the considerably larger total, organic and inorganic P concentrations in the latter. This finding can be explained by the pH in the Sand being ~0.75 pH-units lower than that of the Loam, which may have improved the availability of sorbed P (Barrow, 2017; Eriksson et al., 2016; Kreuzeder et al., 2018; Weng et al., 2011). This is consistent with the higher NH_4Cl-extractable inorganic P present in the Sand (Table 2).

Rhizosphere pH in the Sand increased compared to the bulk soil, which, in accordance with theory and experimental evidence (Barrow, 2017), should decrease P solubility and uptake in plants on P deficient soils. This could explain why, apart from the initially larger P availability indicated by DGT flux and NH_4Cl-extractable P in the bulk soil, the overall shoot P content did not exceed that of the plants grown in the Loam soil. It appears that the observed pH increase in the Sand was related to OH^- or carboxylate efflux for balancing e.g. nitrate and sulphate uptake for maintaining the cellular anion-cation balance (Hinsinger et al., 2003; Loss et al., 1994; Chen et al., 2013; Custos et al., 2020), which is supported by the higher sulphur content in lupins grown on the Sand.

4.2. Phosphorus depletion and phosphatase activity patterns in the rhizosphere

Phosphorus flux images from both soils showed the depletion of DGT-available P along the roots, which agrees with previous studies (Kreuzeder et al., 2018; Santner et al., 2012). These depletion zones indicated P uptake by roots. Apart from one root tip in the Sand soil (Root 1, in 'Sand' panel of Fig. 2) and in contrast to Kreuzeder et al. (2018), who found increased P fluxes around root apices of white lupin, we did not observe clear features of increased P flux and co-solubilised Al, Fe or Ca fluxes (data not shown) which could be indicative for rhizosphere P mobilisation by carboxylates or protons (Hinsinger et al., 2003; Jones, 1998) within the DGT region of interest.

Zones of co-localised P depletion and elevated phosphatase activity were generally associated with visible roots. Profiles across the roots showed that both P depletion and high phosphatase activity extended up to 2 mm into the rhizosphere. However, phosphatases are fairly immobile in soil due to their large molecular weight and strong sorption on soil (Kuzyakov and Razavi, 2019). We observed P depletion but no increased phosphatase activity if the roots were just below the soil surface (cf. Root 1 in the 'Sand' panel in Fig. 2). This indicates that P depletion zones can extend beyond the effect of the phosphatase enzymes, especially at older root parts where P-depletion occurred for a longer period. We also found increasing phosphatase activity from the tip towards the root hair zone (e.g. profiles along the root in Fig. 3), which agrees with previous studies that have highlighted the role of root hairs in enzyme release (Giles et al., 2018; Holz et al., 2020; Ma et al., 2018b; Razavi et al., 2016).

Although the lateral phosphatase activity profiles were comparable in both soils, the phosphatase activity patterns differed between the soils. In the Loam, phosphatase activity was uniformly distributed along all visible roots, which was also reported for other leguminous plants, e.g. lentil and *Lupinus polyphyllus* L., by Razavi et al. (2017, 2016) and Ma et al. (2018a, 2018b). Razavi et al. (2016) suggested that enzyme release follows the general pattern of rhizodeposition and is connected to the P uptake which occurs along the root. In contrast to the Loam, increased phosphatase activity was not observed near all the roots in the Sand, specifically around the tap roots we observed less phosphatase activity while some lateral roots showed very pronounced phosphatase activity. Similar phosphatase distributions were also found by Ma et al. (2018a, 2018b) who demonstrated that lateral roots show higher enzyme activity per unit surface area and affect a larger rhizosphere volume compared to tap roots. While enzyme production to hydrolyse phosphate from organic sources could be more beneficial in the soil containing more organic P (i.e. Loam), roots in the Sand might have focused enzyme production only to lateral roots and invested more in other mobilisation mechanisms, e.g. carboxylates. Even though *Lupinus angustifolius* does not form cluster roots, pronounced release of citrate along the whole root system to cope with nutrient deficiency was observed by several authors (e.g. Egle et al., 1999; Chen et al., 2013; Nuruzzaman et al., 2005b). Due to the cytosolic pH of ~7.3, carboxylic acids are mostly present in their dissociated form (malate, citrate, oxalate) and their exudation is mostly accompanied by cation release (e.g. protons, K^+). Carboxylate anions can react with free protons in soil solution and hence buffer rhizosphere acidification and even increase rhizosphere pH (Hinsinger et al., 2003), which could be another explanation for the greater increase in rhizosphere pH in the more acidic Sand than in the Loam.

Despite the larger organic P pools in the Loam and homogenously distributed high enzyme activity along all roots, P uptake in the Loam did not exceed P uptake in the Sand. This can be explained by the low amount of available inorganic P in the Loam, as reflected by the lower DGT-labile P and NH_4Cl-extractable P. Moreover, in the Loam the mobilization of P esters, i.e. desorption from the soil solid phase rather than the hydrolysis of P esters could have limited P acquisition form organic P pools (Gerke, 2015). The availability of dissolved organic P

has been linked to the limitation of the plant ability to utilize P from organic sources, as enzymatic hydrolysis of P esters is expected to occur in the soil solution rather than on the soil solid phase (Adams and Pate, 1992; Gerke, 2015). While the release of carboxylate ions can be an important mechanism for desorbing inorganic as well as organic P from soil particles to increase their availability (Lambers et al., 2013), oxalate and citrate are known to chelate metals such as Fe, Al and Ca in metal-organic complexes to destabilise large soil organic matter molecules and expose new surfaces for subsequent enzyme-driven hydrolysis (Clarholm et al., 2015). In a strongly P-binding soil, such as the Loam in this study, a further mobilisation mechanism to desorb P esters would seem to be necessary before phosphatases can provide more phosphate from P esters (Gerke, 2015).

4.3. Combined zymography-DGT imaging approach – methodological challenges and perspectives

Combining DGT imaging with zymography is technically well feasible and allows (semi-)quantitative measurements of enzyme activity and element flux distributions at sub-mm resolution. Both imaging methods are non-destructive and hence allow for the visualisation of multiple characteristics in the same soil region, e.g. studying labile element fluxes and enzyme activity patterns at different plant growth stages (Ma et al., 2018a). These observations of the same root within the same soil environment are not possible with common methods where the collection of soil is necessary. However, being non-destructive does not imply that the methods are non-invasive. Hydrolysis of MU-substrates and MU diffusion occurs in the soil even hours after introducing MU-substrate via the zymography membrane and after its removal (Guber et al., 2018). Zymography assessments that rely on MU-substrates (e.g. phosphatase, glucosidase, cellobiosidase, xylanase, chitinase) can hence influence each other in consecutive assessments, as MU from the previous assay can thus induce fluorescence in the subsequent assay although it was not specific to the targeted enzyme (Guber et al., 2018; Razavi et al., 2019).

Combining zymography and DGT raises the question if they can influence each other. The MU-phosphate from the zymography membrane represents an input of P and might influence P measured by DGT. The membrane in this study will have introduced about 3.7 μg cm^{-2} P to the soil surface. If the entire amount of MU-phosphate had diffused from the membrane into the soil and affected the soil within a 1-mm layer, the maximal fertilisation would correspond to 34 mg P kg^{-1}. Even though we can expect substantial losses of MU-phosphate within the agarose gel and the P amounts on the DGT gels were low, we cannot rule out possible effects of zymography on DGT-P. Thus, for future studies we propose to conduct the DGT sampling before zymography and to keep the water content constant at field capacity. Conducting the DGT assay before zymography has the advantage that the time between the end of DGT sampling and the end of the zymography assay is shorter and root growth between the two assays is minimized which simplifies co-localisation of the obtained images.

Fluorescence interferences also need to be considered for accurate zymography interpretation. Organic substances in the soil can either enhance or inhibit fluorescence. Some organic compounds such as quinones fluoresce under UV light (Cory and McKnight, 2005; Del Vecchio et al., 2017). Another issue is that high concentrations of dissolved organic substances such as phenols can also reduce the fluorescence due to quenching effects (Freeman et al., 1995) or because humic substances might cause discoloration of the white zymography membrane, resulting in a lower background signal irrespective of fluorescence. Photographing white membranes under UV light does not allow to differentiate between reflection and fluorescence light at very low MU fluorescence intensities, corresponding to very low background enzyme activities. In the current study, grey values in the Loam bulk soil were lower than the calibration blank, i.e. the white membrane soaked in buffer but without fluorescent MU. A possible explanation for this could be high dissolved organic matter (DOM) release from the Loam that may have inhibited the background signal of the white membrane. While we did not measure soil DOM concentrations, this is supported by our observations of initially transparent DGT gels that were darker after contact with the Loam compared to the Sand, which is probably an effect of DOM diffusing and staining the DGT gels.

For coupling DGT and zymography in future experiments it should be considered that both methods work at 60–80% of the soil water holding capacity (Hooda et al., 1999; Razavi et al., 2019; Santner et al., 2012), so saturation between the assessments is not necessary. Furthermore, zymography membrane filters should be applied directly to the soil surface as described in Razavi et al. (2019, 2016) to reduce lateral diffusion within the agarose gel which could lead to overestimation of the enzyme activity extension (Sanaullah et al., 2016). After the first assessment, soil particles adhering to the membrane or gel might be removed together with the membrane (Guber et al., 2018; Razavi et al., 2019). As both methods rely on good soil-probe contact for diffusion, this could negatively affect the subsequent assessment as gaps and air bubbles result in blind spots on the resulting images that need to be excluded from data analysis (compare red arrows indicating black areas caused by air bubbles in DGT images in Fig. 2). In this study the thin Nuclepore membrane protected the soil surface and the roots during probe handling of both assays.

Quantitative interpretation and relation of the enzyme activity assessed by zymography to DGT-measured flux of available P is limited to relative comparisons of treatments rather than absolute terms. We aimed to quantify localized mechanisms of P mobilisation and associated phosphatase activity in the rhizosphere of blue lupin, but this was not possible in absolute terms as the amount of substrate-P hydrolysed by enzymes measured by zymography cannot be directly related to absolute values of DGT-labile P. Enzyme activity assessed by zymography underestimated the actual enzyme activity because only a fraction of the MU-phosphate that is hydrolysed to MU is detected on the zymography membrane due to substantial diffusional losses of substrate and the product MU (Guber et al., 2018). In this study these losses were even larger due to the agarose gel. Furthermore, the methods are representative of different measurement periods. Zymography represented the amount of substrate hydrolysed and its diffusion within 40 min while the DGT assay accounted for the flux of labile P_i and P_o compounds over 24h. Moreover, enzyme-driven hydrolysis was expected to result in phosphate that would be taken up by roots and accumulate on DGT gels, and depletion of organic P. ZrOH-groups in the DGT gel can bind $HPO_4^{2-}/H_2PO_4^-$ ions but also organic P compounds, even though they have lower diffusion coefficients (Vogel et al., 2019) and hence accumulate to a lesser extent within the given DGT deployment time. However, we cannot draw any conclusions on inorganic and organic P fractions because we only analysed total P that accumulated on the DGT gel by laser-ablation ICP-MS.

To better elucidate the rapid P dynamics in the rhizosphere, DGT could be combined with spectroscopic techniques to determine P species as described by Vogel et al. (2019). To determine the efficiency of phosphatase enzymes and to distinguish between rhizosphere P mobilisation processes, autoradiography of DGT gels could be a promising approach to investigate the fate of ^{33}P-labelled organic P. Furthermore, other elements involved in P solubilisation mechanisms, e.g. Fe and Mn, can be simultaneously mapped by DGT gels (Kreuzeder et al., 2018, 2013) and used to indicate dissolution of P-bearing minerals or co-solubilisation by organic acids (Lambers et al., 2013). Additionally, zymography and DGT could be combined with pH-sensitive planar optical sensors which visualise rhizosphere pH distribution seems promising to gain a more holistic picture of rhizosphere processes.

5. Conclusions

For the first time, we combined zymography and DGT to demonstrate how these powerful techniques can be coupled to observe rhizosphere

processes. The combined approach is technically well feasible and allows (semi-)quantitative measurements of enzyme activity and element flux distributions in the same soil region. Irrespective of P pools and organic matter content of the soils investigated, acid phosphatase activity was similar in both rhizospheres, evidently higher in the rhizosphere as compared to bulk soil, and co-localised with P-depletion zones around the roots. Diffusion-based labile solute sampling by DGT showed that P did not accumulate in labile pools in the rhizosphere. Our results hence suggest that the P uptake rate by the plants was higher than what could be compensated for by enzyme-catalysed mineralisation of organic sources during the deployment. Hydrolysis of P esters seemed to be limited by the low availability of organic P sources hence explaining the similar P uptake in both soils, despite the larger P pools in the Loam. The complex interplay of multiple rhizosphere processes underlines the need for combining different methods to develop novel insight into P acquisition processes by plants. For further studies coupling DGT with zymography methods we recommend conducting DGT assays prior to zymography assays.

Declaration of competing interest

The authors declare that they have no known competing financial interests or personal relationships that could have appeared to influence the work reported in this paper.

Acknowledgements

The authors want to thank Gabrielle Daudin for her help with image processing in ImageJ Fiji, Dr. Christoph Höfer for sharing his knowledge about DGT imaging and providing Excel macros for data processing. This work was supported by the NÖ Forschungs- und Bildungsges.m.b.H. (SC17-015).

Appendix A. Supplementary data

Supplementary data to this article can be found online at https://doi.org/10.1016/j.soilbio.2020.107963.

References

Adams, M.A., Pate, J.S., 1992. Availability of organic and inorganic forms of phosphorus to iupins (Lupinus spp.). Plant Soil 145, 107–113. https://doi.org/10.1007/bf00009546.

Barrow, N.J., 2017. The effects of pH on phosphate uptake from the soil. Plant Soil 410, 401–410. https://doi.org/10.1007/s11104-016-3008-9.

Bhat, K.K.S., Nye, P.H., 1973. Diffusion of phosphate to plant roots in soil. Plant Soil 38, 13. https://doi.org/10.1007/BF00011224.

Boitt, G., Tian, J., Black, A., Wakelin, S.A., Condron, L.M., 2018. Effects of long-term irrigation on soil phosphorus under temperate grazed pasture: irrigation and soil phosphorus. Eur. J. Soil Sci. 69, 95–102. https://doi.org/10.1111/ejss.12512.

Chen, Y.L., Dunabin, V., Diggle, A.J., Siddique, K.H.M., Rengel, Z., 2013. Phosphorus starvation boosts carboxylate secretion in P-deficient genotypes of Lupinus angustifolius with contrasting root structure. Crop Pasture Sci 64, 588–599. https://doi.org/10.1071/CP13012.

Clarholm, M., Skyllberg, U., Rosling, A., 2015. Organic acid induced release of nutrients from metal-stabilized soil organic matter – the unbutton model. Soil Biol. Biochem. 84, 168–176. https://doi.org/10.1016/j.soilbio.2015.02.019.

Custos, J.-M., Moyne, C., Sterckeman, T., 2020. How root nutrient uptake affects rhizosphere pH: a modelling study. Geoderma 369, 114314. https://doi.org/10.1016/j.geoderma.2020.114314.

Condron, L.M., Cornforth, I.S., Davis, M.R., Newman, R.H., 1996. Influence of conifers on the forms of phosphorus in selected New Zealand grassland soils. Biol. Fertil. Soils 21, 37–42. https://doi.org/10.1007/BF00335991.

Cory, R.M., McKnight, D.M., 2005. Fluorescence spectroscopy reveals ubiquitous presence of oxidized and reduced quinones in dissolved organic matter. Environ. Sci. Technol. 39, 8142–8149. https://doi.org/10.1021/es0506962.

Del Vecchio, R., Schendorf, T.M., Blough, N.V., 2017. Contribution of quinones and ketones/aldehydes to the optical properties of humic substances (HS) and chromophoric dissolved organic matter (CDOM). Environ. Sci. Technol. 51, 13624–13632. https://doi.org/10.1021/acs.est.7b04172.

Dick, W.A., Tabatabai, M.A., 1977. Determination of orthophosphate in aqueous solutions containing labile organic and inorganic phosphorus Compounds1. J. Environ. Quality 6, 82–85. https://doi.org/10.2134/jeq1977.00472425000600010018x.

Egle, K., Römer, W., Gerke, J., Keller, H., 1999. The influence of P nutrition on organic acids exudation of roots in three lupin species. In: Van Santen, E., Wink, M., Weissmann, S., Römer, P. (Eds.), Lupin. An Ancient Crop for a New Millenium, New Zealand, pp. 249–251.

Eriksson, A.K., Hesterberg, D., Klysubun, W., Gustafsson, J.P., 2016. Phosphorus dynamics in Swedish agricultural soils as influenced by fertilization and mineralogical properties: insights gained from batch experiments and XANES spectroscopy. Sci. Total Environ. 566–567, 1410–1419. https://doi.org/10.1016/j.scitotenv.2016.05.225.

Freeman, C., Liska, G., Ostle, N.J., Jones, S.E., Lock, M.A., 1995. The use of fluorogenic substrates for measuring enzyme activity in peatlands. Plant Soil 175, 147–152.

George, T.S., Giles, C.D., Menezes-Blackburn, D., Condron, L.M., Gama-Rodrigues, A.C., Jaisi, D., Lang, F., Neal, A.L., Stutter, M.I., Almeida, D.S., Bol, R., Cabugao, K.G., Celi, L., Cotner, J.B., Feng, G., Goll, D.S., Hallama, M., Krueger, J., Plassard, C., Rosling, A., Darch, T., Fraser, T., Giesler, R., Richardson, A.E., Tamburini, F., Shand, C.A., Lumsdon, D.G., Zhang, H., Blackwell, M.S.A., Wearing, C., Mezeli, M. M., Almås, Å.R., Audette, Y., Bertrand, I., Beyhaut, E., Boitt, G., Bradshaw, N., Brearley, C.A., Bruulsema, T.W., Ciais, P., Cozzolino, V., Duran, P.C., Mora, M.L., de Menezes, A.B., Dodd, R.J., Dunfield, K., Engl, C., Frazão, J.J., Garland, G., González Jiménez, J.L., Graca, J., Granger, S.J., Harrison, A.F., Heuck, C., Hou, E.Q., Johnes, P.J., Kaiser, K., Kjær, H.A., Klumpp, E., Lamb, A.L., Macintosh, K.A., Mackay, E.B., McGrath, J., McIntyre, C., McLaren, T., Mészáros, E., Missong, A., Mooshammer, M., Negrón, C.P., Nelson, L.A., Pfahler, V., Poblete-Grant, P., Randall, M., Seguel, A., Seth, K., Smith, A.C., Smits, M.M., Sobarzo, J.A., Spohn, M., Tawaraya, K., Tibbett, M., Voroney, P., Wallander, H., Wang, L., Wasaki, J., Haygarth, P.M., 2018. Organic phosphorus in the terrestrial environment: a perspective on the state of the art and future priorities. Plant Soil 427, 191–208. https://doi.org/10.1007/s11104-017-3391-x.

George, T.S., Richardson, A.E., Simpson, R.J., 2005. Behaviour of plant-derived extracellular phytase upon addition to soil. Soil Biol. Biochem. 37, 977–988. https://doi.org/10.1016/j.soilbio.2004.10.016.

Gerke, J., 2015. The acquisition of phosphate by higher plants: effect of carboxylate release by the roots. A critical review. J. Plant Nutr. Soil Sci. 178, 351–364. https://doi.org/10.1002/jpln.201400590.

Giles, C.D., Dupuy, L., Boitt, G., Brown, L.K., Condron, L.M., Darch, T., Blackwell, M.S.A., Menezes-Blackburn, D., Shand, C.A., Stutter, M.I., Lumsdon, D.G., Wendler, R., Cooper, P., Wearing, C., Zhang, H., Haygarth, P.M., George, T.S., 2018. Root development impacts on the distribution of phosphatase activity: improvements in quantification using soil zymography. Soil Biol. Biochem. 116, 158–166. https://doi.org/10.1016/j.soilbio.2017.08.011.

Guber, A., Kravchenko, A., Razavi, B.S., Uteau, D., Peth, S., Blagodatskaya, E., Kuzyakov, Y., 2018. Quantitative soil zymography: mechanisms, processes of substrate and enzyme diffusion in porous media. Soil Biol. Biochem. 127, 156–167. https://doi.org/10.1016/j.soilbio.2018.09.030.

Heitkötter, J., Marschner, B., 2018. Soil zymography as a powerful tool for exploring hotspots and substrate limitation in undisturbed subsoil. Soil Biol. Biochem. 124, 210–217. https://doi.org/10.1016/j.soilbio.2018.06.021.

Hendrie, D.L., Moir, J.L., Stevens, E.J., Black, A.D., Moot, D.J., 2018. Soil pH, exchangeable aluminium and legume yield responses to deep-placed lime at Omarama Station. J. New Zealand Grasslands 137–144. https://doi.org/10.33584/jnzg.2018.80.341.

Hinsinger, P., Plassard, C., Tang, C., Jaillard, B., 2003. Origins of root-mediated pH changes in the rhizosphere and their responses to environmental constraints: a review. Plant Soil 248, 43–59. https://doi.org/10.1023/A:1022371130939.

Holz, M., Zarebanadkouki, M., Carminati, A., Becker, J.N., Spohn, M., 2020. The effect of root hairs on rhizosphere phosphatase activity. J. Plant Nutr. Soil Sci. https://doi.org/10.1002/jpln.201900426.

Hooda, P.S., Zhang, H., Davison, W., Edwards, A.C., 1999. Measuring bioavailable trace metals by diffusive gradients in thin films (DGT): soil moisture effects on its performance in soils. Eur. J. Soil Sci. 50, 285–294. https://doi.org/10.1046/j.1365-2389.1999.00226.x.

Jones, D.L., 1998. Organic acids in the rhizosphere – a critical review. Plant Soil 205, 25–44.

Kreuzeder, A., Santner, J., Prohaska, T., Wenzel, W.W., 2013. Gel for simultaneous chemical imaging of anionic and cationic solutes using diffusive gradients in thin films. Analytical Chem. 85, 12028–12036. https://doi.org/10.1021/ac403050f.

Kreuzeder, A., Santner, J., Scharsching, V., Oburger, E., Hoefer, C., Hann, S., Wenzel, W. W., 2018. In situ observation of localized, sub-mm scale changes of phosphorus biogeochemistry in the rhizosphere. Plant Soil 424, 573–589. https://doi.org/10.1007/s11104-017-3542-0.

Kuzyakov, Y., Razavi, B.S., 2019. Rhizosphere size and shape: temporal dynamics and spatial stationarity. Soil Biol. Biochem. https://doi.org/10.1016/j.soilbio.2019.05.011. S0038071719301452.

Lambers, H., Clements, J.C., Nelson, M.N., 2013. How a phosphorus-acquisition strategy based on carboxylate exudation powers the success and agronomic potential of lupines (*Lupinus* , Fabaceae). Am. J. Bot. 100, 263–288. https://doi.org/10.3732/ajb.1200474.

Loss, S.P., Robson, A.D., Ritchie, G.S.P., 1994. Nutrient uptake and organic acid anion metabolism in lupins and peas supplied with nitrate. Annals Bot. 74, 69–74. https://doi.org/10.1093/aob/74.1.69.

Ma, X., Liu, Y., Zarebanadkouki, M., Razavi, B.S., Blagodatskaya, E., Kuzyakov, Y., 2018a. Spatiotemporal patterns of enzyme activities in the rhizosphere: effects of plant growth and root morphology. Biol. Fertil. Soils 54, 819–828. https://doi.org/10.1007/s00374-018-1305-6.

Ma, X., Zarebanadkouki, M., Kuzyakov, Y., Blagodatskaya, E., Pausch, J., Razavi, B.S., 2018b. Spatial patterns of enzyme activities in the rhizosphere: effects of root hairs

and root radius. Soil Biol. Biochem. 118, 69–78. https://doi.org/10.1016/j.soilbio.2017.12.009.

Mat Hassan, H., Marschner, P., McNeill, A., Tang, C., 2012. Growth, P uptake in grain legumes and changes in rhizosphere soil P pools. Biol. Fertil. Soils 48, 151–159. https://doi.org/10.1007/s00374-011-0612-y.

Menezes-Blackburn, D., Giles, C., Darch, T., George, T.S., Blackwell, M., Stutter, M., Shand, C., Lumsdon, D., Cooper, P., Wendler, R., Brown, L., Almeida, D.S., Wearing, C., Zhang, H., Haygarth, P.M., 2018. Opportunities for mobilizing recalcitrant phosphorus from agricultural soils: a review. Plant Soil 427, 5–16. https://doi.org/10.1007/s11104-017-3362-2.

Nash, D.M., Haygarth, P.M., Turner, B.L., Condron, L.M., McDowell, R.W., Richardson, A.E., Watkins, M., Heaven, M.W., 2014. Using organic phosphorus to sustain pasture productivity: a perspective. Geoderma 221–222, 11–19. https://doi.org/10.1016/j.geoderma.2013.12.004.

Nuruzzaman, M., Lambers, H., Bolland, M.D., Veneklaas, E.J., 2005a. Phosphorus benefits of different legume crops to subsequent wheat grown in different soils of Western Australia. Plant Soil 271, 175–187. https://doi.org/10.1007/s11104-004-2386-6.

Nuruzzaman, M., Lambers, H., Bolland, M.D.A., Veneklaas, E.J., 2005b. Phosphorus uptake by grain legumes and subsequently grown wheat at different levels of residual phosphorus fertiliser. Austr. J. Agricultural Res. 56, 1041. https://doi.org/10.1071/AR05060.

Razavi, B.S., Hoang, D.T.T., Blagodatskaya, E., Kuzyakov, Y., 2017. Mapping the footprint of nematodes in the rhizosphere: cluster root formation and spatial distribution of enzyme activities. Soil Biol. Biochem. 115, 213–220. https://doi.org/10.1016/j.soilbio.2017.08.027.

Razavi, B.S., Zarebanadkouki, M., Blagodatskaya, E., Kuzyakov, Y., 2016. Rhizosphere shape of lentil and maize: spatial distribution of enzyme activities. Soil Biol. Biochem. 96, 229–237. https://doi.org/10.1016/j.soilbio.2016.02.020.

Razavi, B.S., Zhang, X., Bilyera, N., Guber, A., Zarebanadkouki, M., 2019. Soil zymography: simple and reliable? Review of current knowledge and optimization of the method. Rhizosphere 11, 100161. https://doi.org/10.1016/j.rhisph.2019.100161.

Sanaullah, M., Razavi, B.S., Blagodatskaya, E., Kuzyakov, Y., 2016. Spatial distribution and catalytic mechanisms of β-glucosidase activity at the root-soil interface. Biol. Fertil. Soils 52, 505–514. https://doi.org/10.1007/s00374-016-1094-8.

Santner, J., Zhang, H., Leitner, D., Schnepf, A., Prohaska, T., Puschenreiter, M., Wenzel, W.W., 2012. High-resolution chemical imaging of labile phosphorus in the rhizosphere of Brassica napus L. cultivars. Environ. Exp. Bot. 77, 219–226. https://doi.org/10.1016/j.envexpbot.2011.11.026.

Scanlan, C., 2015. Diagnosing phosphorus deficiency in narrow-leafed lupins [WWW Document]. https://www.agric.wa.gov.au/mycrop/diagnosing-phosphorus-deficiency-narrow-leafed-lupins. accessed 7.19.20.

Schindelin, J., Arganda-Carreras, I., Frise, E., Kaynig, V., Longair, M., Pietzsch, T., Preibisch, S., Rueden, C., Saalfeld, S., Schmid, B., Tinevez, J.-Y., White, D.J., Hartenstein, V., Eliceiri, K., Tomancak, P., Cardona, A., 2012. Fiji: an open-source platform for biological-image analysis. Nature Methods 9, 676–682. https://doi.org/10.1038/nmeth.2019.

Shen, J., Yuan, L., Zhang, J., Li, H., Bai, Z., Chen, X., Zhang, W., Zhang, F., 2011. Phosphorus dynamics: from soil to plant. Plant Physiol. 156, 997–1005. https://doi.org/10.1104/pp.111.175232.

Spohn, M., Carminati, A., Kuzyakov, Y., 2013. Soil zymography – a novel in situ method for mapping distribution of enzyme activity in soil. Soil Biol. Biochem. 58, 275–280. https://doi.org/10.1016/j.soilbio.2012.12.004.

Tate, K.R., Giltrap, D.J., Claydon, J.J., Newsome, P.F., Atkinson, I.A.E., Taylor, M.D., Lee, R., 1997. Organic carbon stocks in New Zealand's terrestrial ecosystems. J. Roy. Soc. New Zeal. 27, 315–335. https://doi.org/10.1080/03014223.1997.9517541.

Turner, B.L., Wells, A., Andersen, K.M., Condron, L.M., 2012. Patterns of tree community composition along a coastal dune chronosequence in lowland temperate rain forest in New Zealand. Plant Ecol. 213, 1525–1541. https://doi.org/10.1007/s11258-012-0108-3.

Vogel, C., Sekine, R., Steckenmesser, D., Lombi, E., Herzel, H., Zuin, L., Wang, D., Félix, R., Adam, C., 2019. Combining diffusive gradients in thin films (DGT) and spectroscopic techniques for the determination of phosphorus species in soils. Analytica Chimica. Acta. https://doi.org/10.1016/j.aca.2019.01.037. S0003267019301229.

Wagner, S., Hoefer, C., Puschenreiter, M., Wenzel, W.W., Oburger, E., Hann, S., Robinson, B., Kretzschmar, R., Santner, J., 2020. Arsenic redox transformations and cycling in the rhizosphere of Pteris vittata and Pteris quadriaurita. Environ. Exp. Bot. 177, 104122. https://doi.org/10.1016/j.envexpbot.2020.104122.

Weng, L., Vega, F.A., Van Riemsdijk, W.H., 2011. Competitive and synergistic effects in pH dependent phosphate adsorption in soils: LCD modeling. Environ. Sci. Technol. 45, 8420–8428. https://doi.org/10.1021/es201844d.

Whitley, A.E., Moir, J.L., Almond, P.C., Moot, D.J., 2016. Soil pH and exchangeable aluminium in contrasting New Zealand high and hill country soils. Hill Country – Grassland Res. Pract. 16, 169–172.

Zhang, X., Dippold, M.A., Kuzyakov, Y., Razavi, B.S., 2019. Spatial pattern of enzyme activities depends on root exudate composition. Soil Biol. Biochem. 133, 83–93. https://doi.org/10.1016/j.soilbio.2019.02.010.